

Analysis of the electron density features of small boron clusters and the effects of doping with C, P, Al, Si, and Zn: Magic B₇P and B₈Si clusters

P. Saha^a, A. B. Rahane^b, V. Kumar^{b,c} and N. Sukumar^{a,c}

^a*Department of Chemistry, School of Natural Sciences, Shiv Nadar University, NH-91, Tehsil Dadri, Gautam Budhha Nagar 201314, Uttar Pradesh, India*

^b*Dr. Vijay Kumar Foundation, 1969, Sector 4, Gurgaon-122 001, Haryana, India,*

^c*Center for Informatics, School of Natural Sciences, Shiv Nadar University, NH-91, Tehsil Dadri, Gautam Budhha Nagar 201314, Uttar Pradesh, India*

Corresponding Author E-mail: n.sukumar@snu.edu.in

Abstract

Boron atomic clusters show several interesting and unusual size-dependent features due to the small covalent radius, electron deficiency, and higher coordination number of boron as compared to carbon. These include aromaticity and a diverse array of structures such as quasi-planar, ring or tubular shaped, and fullerene-like. In the present work, we have analyzed features of the computed electron density distributions of small boron clusters having up to 11 boron atoms, and investigated the effect of doping with C, P, Al, Si, and Zn atoms on their structural and physical properties, in order to understand the bonding characteristics and discern trends in bonding and stability. We find that in general there are covalent bonds as well as delocalized charge distribution in these clusters. We associate the strong stability of some of these planar/quasiplanar disc-type clusters with the electronic shell closing with effectively twelve delocalized valence electrons using a disc-shaped jellium model. B₉⁻, B₁₀, B₇P, and B₈Si, in particular, are found to be exceptional with very large gaps between the highest occupied molecular orbital (HOMO) and the lowest unoccupied molecular orbital (LUMO), and these are suggested to be magic clusters.

1. Introduction

There have been exciting developments in recent years related to nanostructures of boron that could lead to novel forms and new structures of boron. Boron nanoclusters have been found to exist in a variety of structures. Small clusters have planar or quasi-planar structures and even for a relatively large cluster B_{84} a quasi-planar structure has been found [1] to have the lowest energy. For some sizes tubular structures become favorable, and in some other cases such as B_{40} , a fullerene-like cage structure [2] has the lowest energy. Stuffed or core-shell structures have also been found [3] such as for B_{28} , B_{68} , and B_{74} while ring structures have been reported for small boron clusters with a metal atom [4]. A new phase of boron has also been found [5] under pressure in which coexistence of two kinds of clusters with quite different properties lead to a significant internal charge transfer between the clusters and to a quite unusual partly ionic elemental phase. Several experimental and theoretical studies have led to an understanding of the structures of many small and mid-size boron clusters having less than 50 atoms [6], but much is yet to be understood as there is still no clear trend on the growth behavior of boron clusters. Quasi-planar, tubular, and cage structures compete in energy, and charging the clusters (anion/cation) sometimes changes the energy ordering of isomers. This opens up the opportunity to develop new structures of boron by doping. Further, the nature of bonding in small boron clusters still remains open. Two center (2c), three center (3c), and multi-center bonding have been suggested in boron clusters by using adaptive natural density partitioning (AdNDP) [7] analysis. Here we use electron density critical point analysis to understand the nature of bonding in small boron clusters, supplemented by ELF (electron localization function) and AdNDP analysis. We also study the effect of doping with different hetero atoms, to show that disk-like structures of boron can be created with electronic shell closing at effectively 12 delocalized valence electrons.

Boron provides a test bed for concepts of bonding in molecules. Several distinct conceptions of the chemical bond can be distinguished:

- A chemical bond may be considered as a force that holds pairs of atoms together, and is manifested in the energy required to break the bond (dissociation energy).
- This is related to, but different from, the Lewis concept [8] of the electron pair bond. The two concepts become identical for a closed shell diatomic molecule, where the dissociation energy correlates directly with the increase in electron density between the nuclei, but the correlation is not as straight-forward for open shell systems or for many polyatomics. Electron pairing is a consequence of the Pauli exclusion principle, the tendency of electrons with the same spin to avoid each other, over and beyond the Coulomb repulsion between all electrons. This is evident from study of the same spin pair density [13, 14]. The Fermi hole is the physical

manifestation of the Pauli exclusion principle: it describes how the density of a reference electron extends into the space of another electron of same spin, thereby excluding an equal amount of same spin density.

- The traditional Lewis electron pair bond concept is inadequate to explain bonding in B₂H₆ and other boranes, and was thus extended by Longuet-Higgins [9], Lipscomb [10] and Massa, *et al* [11] to admit the possibility of 3-center, 2-electron bonds (“banana bonds”) in such molecules.
- This concept of multi-center bonding has subsequently been further extended, using AdNDP analysis, to include n-center, but always 2-electron “objects” (with n arbitrarily large). AdNDP is an extension of natural bond orbitals (NBO) analysis [12], which exploits the invariance of the total electron density, energy and other molecular properties to unitary transformations of the occupied orbitals. In AdNDP, n x n blocks of the one-electron density matrix are diagonalized in a basis of atomic orbitals; eigenvectors with eigenvalues close to two are identified with n-center, 2-electron bonds.
- An alternate view to such orbital treatments is to define atoms and bonds in molecules solely with respect to features of the total electron density, a physically “observable” quantity, in 3-D space. Bader’s bond paths [13], which are gradient paths of the electron density $\nabla\rho(\mathbf{r})$ connecting pairs of nuclei, are topological features of the electron density, but are *not* associated with any definite electron count. Electron counts are obtained by integrating electron density over a volume, *e.g.* the basin of an atom. Being a topological property, the mere existence of a bond path between a pair of nuclei does not say anything about the strength of the chemical bond between the atoms. Bader and coworkers [13, 14] have studied the properties of valence shell charge concentrations, both bonded electrons and non-bonding “lone pairs”, through the negative Laplacian distribution of the electron density $L(\mathbf{r}) = -\nabla^2\rho(\mathbf{r})$. The negative of the Laplacian identifies regions of electron density accumulation ($L > 0$) and depletion ($L < 0$). The bond critical point (BCP) \mathbf{r}_c is the saddle point of the electron density, where the gradient $\nabla\rho(\mathbf{r}_c) = 0$ and $\rho(\mathbf{r}_c)$ is a minimum along the bond path and a maximum in any direction perpendicular to it. The electron density and the Laplacian at the BCP reveal clues to the nature of bonding between the atoms. In a covalent bond, the electron density accumulates in the inter-nuclear region, with a shallow curvature along the bond path and a steep curvature perpendicular to it. Thus $L(\mathbf{r}_c) \gg 0$ for a covalent bond, and such bonds are characterized by large magnitudes of the Coulomb potential energy of attraction between electrons and nuclei in the inter-nuclear region, which forms the classical

part of the binding stabilization. Ionic bonds are characterized by large kinetic energy with very little increase of electron density in the inter-nuclear region, and $L(\mathbf{r}_c) < 0$. Combining topological properties of the electron density with information about the magnitudes of $\rho(\mathbf{r}_c)$ and $L(\mathbf{r}_c)$ thus allows meaningful chemical conclusions about bonding to be drawn. Indeed, Bader and Heard [14] showed that the Laplacian of the electron density is generally homeomorphic to that of the conditional same spin pair density, which locates electron pairs, thus explaining how concentrations of electron density, as identified by the topology of the Laplacian function, also identify electron pairs.

These alternate conceptions of the chemical bond often coincide for closed-shell organic molecules, but can diverge dramatically in the case of “electron deficient” boron compounds and for metallic nanoclusters, where extensive electron delocalization and multi-center bonding are prevalent. It is therefore instructive to examine small systems from a multiplicity of viewpoints, so that the validity and limitations of each approach can be understood. We have carried out such an analysis for small pure boron clusters (neutral as well as anions) and also for doped clusters. We have considered doping of boron clusters with a carbon atom, as such clusters are isoelectronic to the anion boron clusters. We have also studied selected boron clusters doped with Al, Si, P, and Zn atoms. Doping of boron clusters may lead to novel structures, as is the case for metal-doped silicon and other clusters [15]. Recently doping by a Cr, Mo, and W atom has been reported in the literature to stabilize a B_{24} fullerene-like cluster [16]. Furthermore, Bing *et al.* [17] have studied theoretically the atomic structures of aluminum-doped boron clusters with 2 to 9 boron atoms, while Nb doping has been shown to form a wheel structure of $B_{10}Nb$ cluster [18]. Romanescu *et al.* [19] have experimentally and theoretically studied Fe-doped boron ring nanostructures FeB_8 and FeB_9 . They have found that in the ground state both these clusters are doubly aromatic, and that the iron atom interacts with the peripheral boron ring exclusively through delocalized bonds. In this paper we focus on the effects of doping of small boron clusters with C, Al, Si, P, and Zn on their structure and stability.

As the structures of small undoped boron clusters are planar or quasi-planar, it is instructive to consider a circular disk of charge such as in a jellium model, where there occur islands of exceptional stability with 2, 6, 12, 20, ... valence electrons [20]. Such clusters are often called “magic clusters”. As we shall show, boron clusters have localized covalent bonds as well as delocalized π -bonded charge, with the latter behaving like free electrons. We consider boron clusters in the size range of 6 to 10 atoms and dope them with Al, Si, P, and Zn atoms to obtain the doped clusters B_6P_2 , B_7P , B_8Si , B_9Al , and $B_{10}Zn$ in an effort to find clusters with effectively twelve valence electrons. We find large HOMO-LUMO gaps for B_7P and B_8Si as well as increased binding energy by doping, indicating their high stability, which we correlate with the existence of a magic number of 12 valence electrons

following a Jellium model [21].

2. Computational details

The calculations have been performed using density functional theory with generalized gradient approximation (GGA) of Perdew, Burke and Ernzerhof (PBE) [22] for the exchange-correlation energy. The electron-ion interaction is treated with the projector augmented wave (PAW) pseudopotential method [23] using the Vienna *Ab initio* Simulation Package (VASP) [24]. We used medium precision to expand the wavefunction in a plane wave basis. The calculations were considered to be converged when the absolute value of the force on each ion was less than 0.005 eV \AA^{-1} with a convergence for the total energy of about 10^{-5} eV without any symmetry constraint. The gamma point has been used for Brillouin zone integrations. A cubic supercell with lattice parameter of 20 \AA was used for the VASP calculations. Structures of the nanoclusters were also optimized, and IR and Raman spectra calculated using the Gaussian09 package [25] with the B3PW91/6-311G basis set [26]. These are given in in the Supplementary Information. In all cases the lowest energy isomers are found to have real frequencies supporting dynamical stability of the structures. The AIMAll [27] package was used to analyze the gradient paths, critical points and Laplacian distributions of the electron density obtained from the Gaussian09 calculation. Further calculations have been done using the PBE0 exchange-correlation functional and the lowest energy structures remain the same.

3. Results and Discussion

Pure boron clusters:

We first studied pure neutral boron clusters in the size range of 3 to 11 atoms. The optimized atomic structures are shown in Fig. 1, together with the electron density contours, bond paths, BCPs and ring critical points (RCPs). Our results for the low lying structures agree with the results reported earlier [28, 29]. Here we considered only the isomer of the lowest energy in each case. Contours of the Laplacian distribution are shown in Fig. 2. The negative Laplacian of the electron density $L(\mathbf{r}) = -\nabla^2\rho(\mathbf{r})$ identifies regions of electron density accumulation ($L > 0$) that appear as solid contours in Fig. 2, while regions of electron density depletion ($L < 0$) appear as dashed contours. Electron density contours, bond paths, and critical points for the corresponding singly charged anion clusters are shown in Fig. 3, and contours of the Laplacian distribution in Fig. 4. Another measure commonly employed to identify regions of electron density localization is the electron localization function ELF [30], which varies in the range [0,1], with $\text{ELF}=\frac{1}{2}$ corresponding to the uniform electron gas, while the upper limit $\text{ELF}=1$ corresponds to perfect localization. ELF isosurfaces with the value of 0.7 for pure neutral boron clusters B_n are shown for $n = 3-11$ in Fig. 5. Inspection of the Laplacian and ELF distributions reveals strong evidence for electron density localization in peripheral bonds and electron

density delocalization in the interior of the rings over the basins of 3, 4, 5 and even larger numbers of atoms in several clusters. Bifurcation analysis (not shown) reveals features that appear only at low values of ELF, indicating that the charge in these regions is delocalized. Laplacian and ELF analysis do not always agree on the details of multi-center bonding, which is not surprising as these are very different functions [14], but there is general agreement on existence or absence of multi-center bonding, as detailed below.

The bond paths in B_3 and B_3^- (Figs. 1 and 2 and Table S1 in Supplementary Information) show pronounced curvature and ellipticity. Bond ellipticity is a quantitative measure of the deviation of the electron density distribution from cylindrical symmetry, and is related to the ratio of the two positive eigenvalues of L at the BCP; ellipticity is close to zero for a conventional sigma bond. It may be noted that the bond paths in B_3 and B_3^- curve inwards (opposite to the situation in cyclopropane and cyclopropene, where the bond paths curve outwards), a consequence of the electron deficient nature of the ring, resulting in all three atoms sharing the available electrons. This is also reflected in ELF isosurfaces of B_3 and B_3^- (Fig. 5) which do not show localization of charge along a bond.

B_4 and B_4^- have symmetry-broken ring structures, with unequal diagonals. The two closer atoms have a higher integrated electron density in their basins, and thus more negative charge (-0.175 in B_4 and -0.35 in B_4^-) than the atoms that are farther away (+0.175 in B_4 and -0.15 in B_4^-). The single RCP in B_4 splits into two RCPs and one BCP in B_4^- with the appearance of a ridge of electron density (bond path) along the shorter diagonal. However, the electron density at this new BCP (0.132 e/Bohr^3 , Table S1(b) in Supplementary Information) is not noticeably different from that of the RCPs, and the bridging bond has an unusually high ellipticity. In other words, the electron density is rather flat in the interior of the two rings, and may thus legitimately be considered as being shared among all four atoms, rather than forming a conventional two-center bridging bond. ELF analysis (Fig. 5) lends support to this point of view. The positive contours of L (signifying electron density accumulation) in the centers of the rings in B_5^- , B_6 , and B_6^- (Figs. 2 and 4) are also interpreted as evidence for multi-center bonding in these molecules. The electron density at the RCP falls steadily with increase in ring size, and L becomes steadily more negative. This is again in agreement with the ELF isosurfaces (Fig. 5). A similar behavior of ELF is seen for B_5 , B_5^- , B_6 , and B_6^- again supporting the conclusion based on the results of L . The existence of three-center bonding in B_5^- as opposed to B_5 is supported both by the appearance of positive contours of L and by ELF isosurfaces between three atoms.

The 7-, 8-, and 9-atom boron clusters adopt wheel-like structures, with one boron atom occupying the center. In each of these clusters, the peripheral bonds have much higher $\rho(\mathbf{r}_c)$ and $L(\mathbf{r}_c)$ than the radial bonds (Fig. S1 in Supplementary Information), supporting the identification of the former with

conventional 2-center, 2-electron bonds. One can also note positive L contours around the peripheral BCPs. The radial bonds have $\rho(\mathbf{r}_c)$ and $L(\mathbf{r}_c)$ very close to those of the RCPs and large bond ellipticities. The average bond ellipticity of anionic clusters (9.57) is much greater than that of neutral clusters (1.48). In B_7 and B_7^- we also see the appearance of contours of L encompassing two or more RCPs and a BCP (Figs. 3 and 4), supporting an interpretation in terms of 4-center delocalization. The existence of positive contours of L around a RCP between three atoms is also indicative of 3-center bonding. The ELF isosurfaces (Fig. 5) show strong localization of non-bonded charge on central atom in B_8 , B_8^- , B_9 and B_9^- . The 10- and 11-atom clusters are large enough to accommodate two boron atoms within the ring. B_{10} has a ring of eight B atoms and two B atoms inside while in B_{11} one boron atom is added to the ring. In addition to the peripheral and bridging bonds (e.g. bond between the two atoms inside the ring in B_{10} and B_{10}^-), the contours of L (Figs. 3 and 4) and ELF (Fig. 5) provide evidence for electron delocalization encompassing at least 3 or 4 atomic basins and localization of electron density along the periphery of the clusters as well as the bridging bonds.

Topological features in clusters with multiple energy minima can be sensitive to small geometrical distortions and to the details of the basis set and level of theory employed in computations. As already emphasized, the mere existence of a bond path between a pair of atoms does not reveal the strength of the chemical bond between them, and it is necessary to analyze this topological information together with information about the magnitudes of $\rho(\mathbf{r}_c)$ and $L(\mathbf{r}_c)$ before chemically meaningful conclusions may be drawn. The electron density $\rho(\mathbf{r}_c)$ and negative of the Laplacian $L(\mathbf{r}_c)$ at the critical points are linearly inter-correlated for both neutral (Pearson correlation coefficient 0.967 at BCP and 0.862 at RCP) and anionic (Pearson correlation coefficient 0.930 at BCP and 0.899 at RCP) boron clusters (Figure S5 in Supplementary Information). Different classes of BCPs appear in different regions of the figures. The existence of two distinct types of B-B bonds in these clusters is apparent. B-B bonds located at the periphery of the clusters are characterized by relatively high values of electron density and L , as for conventional covalent bonds, whereas the BCPs in the interior of the clusters are not noticeably different from the RCPs in their electron densities. Furthermore, both RCPs and BCPs in the interior of the clusters have L very close to zero. This segregation of bond paths into different classes is even more obvious upon examining each cluster separately (Fig. S1 in Supplementary Information). Several of the interior BCPs also have unusually high bond ellipticities (Fig. S6 in Supplementary Information), indicating that the bond electron density is preferentially distributed in the ring plane. The boron clusters are thus characterized by very flat electron densities within the rings, a fact which is also evident from high ellipticities and from the existence of few contours within the rings in the electron density plots. Notwithstanding the appearance of RCPs and BCPs within the boron rings, the electron density in the interior of these rings forms a system of

delocalized charge over multiple atomic centers.

Interestingly for B_3^- , B_4 , B_9^- , and B_{10} the HOMO-LUMO gaps are large (Table 1) with the GGA values of 3.48 eV, 3.81 eV, 4.12 eV, and 2.98 eV, respectively. The molecular orbitals of B_3^- show that the lowest lying molecular orbital is of s type, followed by three p type molecular orbitals. The HOMO shows the characteristics of a three-center covalent bond. Considering B_9^- and B_{10} , there are effectively twelve delocalized valence electrons, which corresponds to electronic shell closing in a jellium model of a disk, and therefore these are magic clusters. In the case of B_9^- , one finds that each boron atom on the peripheral ring has two electrons covalently bonded with the neighboring boron atoms while one valence electron contributes to the pi bonding (delocalization) in the orbital model. The central boron atom contributes three valence electrons in the orbital model, which together with the extra electron of the anion, adds up to effectively twelve delocalized electrons. For B_{10} , similar to B_9^- , each boron atom on the peripheral ring contributes one delocalized electron, making in total eight delocalized electrons from the peripheral ring, while the two boron atoms inside the ring are covalently bonded, taking away two electrons and leaving four delocalized electrons. All together this amounts to effectively twelve delocalized electrons corresponding to electronic shell closing. The symmetry of this cluster is reduced and therefore the HOMO-LUMO gap is also lower compared with B_9^- . Interestingly B_6^- has a high spin quartet state as the lowest energy state. The energy difference between the quartet and doublet states is 0.1 eV. We have also performed calculations on B_{12} (a triangle of three boron atoms inside a ring of 9 B atoms) and B_{13}^+ (3 B atoms in a ring of 10 B atoms) clusters; both these clusters also have large HOMO-LUMO gaps of 3.63 eV and 3.35 eV, respectively.

Doped clusters:

(a) Carbon doped clusters

Next we studied neutral boron clusters in the same size range, with a single carbon atom replacing a boron at various positions. These clusters are electronically equivalent to anion boron clusters. A few low lying isomers for each cluster size, obtained from VASP calculations, are shown in Fig. 6. Calculations based on the Gaussian program with B3PW91 as well as PBE0 exchange-correlation functional give the same lowest energy isomer. The electron density contours and critical points for the lowest energy isomers, as obtained from the Gaussian program with B3PW91 exchange-correlation functional, are shown in Fig. 7, while the Laplacian distributions are shown in Fig. 8, and the ELF isosurfaces obtained from VASP, in Fig. 9. Comparing the different isomers of carbon-doped neutral boron clusters (Table S1(c) in Supplementary Information), we see that carbon atoms prefer to occupy vertices with low coordination number, and that boron atoms with higher coordination have higher integrated electron populations. Again the electron densities and negative of the Laplacians at

the B-B BCPs are well correlated with each other (Pearson correlation coefficient 0.948, shown in Supplementary Information), but there is no such correlation for B-C bonds. As expected, B-C BCPs have the highest electron densities, and RCPs the least. B-C bonds have somewhat higher bond ellipticities (2.91) than B-B bonds (1.88) in these doped clusters. L in Fig. 8 shows positive contours between atoms on the periphery; as for the pure boron clusters, these represent covalent bonds between the neighboring atoms. This interpretation is consistent with the ELF isosurfaces shown in Fig. 9, where one can see isosurfaces on the peripheral atoms, particularly for B₄C, B₇C, B₈C, and B₉C. Contours of the Laplacian encompassing several atoms represent multi-center bonds or delocalization of charge. The ELF contours in Fig. 9 show strong localization of non-bonded charge on the central atom in B₄C, B₅C, B₇C, B₈C, and B₉C. In Table I we list the HOMO-LUMO gaps of the carbon doped clusters that are similar to the pure anion boron clusters. The HOMO-LUMO gap is large for B₂C and B₈C similar to the cases of B₃⁻ and B₉⁻.

(b) Doping with P, Si, Al, and Zn

The most stable optimized atomic structures and charge density contours of B₆P₂, B₇P, B₈Si, and B₉Al are shown in Fig. 10. The isomer shown in Fig. 10 for B₁₀Zn is one in which Zn substitutes a boron site inside the ring. However, the lowest energy isomer is one in which a Zn atom caps the lowest energy isomer of the B₁₀ cluster. We calculated the doping energy $E_d = E(B_n) + E(M) - E(B_nM)$, where $E(B_n)$, $E(M)$, and $E(B_nM)$ are the energies of the B_n cluster, M atom, and B_nM cluster. It is found that the doping energy is very small (0.033 eV) for Zn and therefore interaction of Zn is very weak, while for B₆P₂, B₇P, B₈Si, and B₉Al, the doping energy is 4.818 eV, 5.55 eV, 5.63 eV, and 4.27 eV, respectively, per boron atom. These results show that B₇P and B₈Si are very good candidates for doped boron clusters. There is significant gain in energy from doping in these two cases, as the binding energy of pure B₇ and B₈ clusters is 4.795 eV/atom and 5.028 eV/atom, respectively, while for B₆ (binding energy 4.738 eV/atom), the gain in energy is small. B₆P₂ exhibits a structure with a distorted ring of six boron atoms and two P atoms capping it on both the sides. This has a large HOMO-LUMO gap of 1.98 eV. B₇P has a hexagonal bipyramidal structure with the P and one B atom capping the hexagon on the two sides. For B₈Si there is a heptagon of boron which is capped with a Si atom on one side and a B atom on the other side while for B₉Al, Al atom occupies a site on the ring. The stability of B₇P is attributed to 12 delocalized valence electrons (six from the hexagonal base of boron atoms, three from the apex boron atom and three *p* electrons from the P atom, *s* electrons being localized on P atom, as also shown later). This corresponds to shell closing in a disk jellium model. This magic cluster has a large HOMO-LUMO gap of 3.29 eV. The integrated electron density in the basin of the P atom is 14.7 electrons, and there is significant charge transfer of 0.53 electrons to the capping B atom, including 0.23 e charge transfer from the base boron atoms. B₈Si has an even

larger HOMO-LUMO gap of 4.30 eV, and it also corresponds to electronic shell closure at 12 valence electrons (seven electrons from the peripheral boron atoms, three from the capping boron atom and two *p* electrons from the Si atom, 3*s* electrons being localized as also shown later). The integrated electron density in the basin of the Si atom is 13.35 electrons, and 0.06 e charge is transferred to each of the base B atoms, while 0.25 e is transferred to the capping B atom. Electron densities and Laplacians at ring and bond critical points of P, Si, Al, and Zn doped neutral boron clusters are shown in Table S1(d) in Supplementary Information. The contour plots of *L* in Fig. 11 show positive contours and covalent bonding between peripheral boron atoms. In the case of the AlB₉ cluster, the Al atom occupies a site at the periphery of the B₁₀ cluster, and the symmetry of the cluster is reduced. This along with changed interactions in the cluster reduces the HOMO-LUMO gap to 1.21 eV. The Al atom transfers 1.33 e to the neighboring four boron atoms, and there is also small charge transfer of about 0.04 e from each of the remaining boron atoms to these boron atoms. The Laplacian contours in Fig. 11 show delocalization of charge, and covalent bonds between neighboring peripheral boron atoms as well as between the two boron atoms inside. The electron density contours for the isomer shown suggest delocalization of charge around the Zn atom. There is a charge transfer of 0.66 e from Zn to some boron atoms.

The IR and Raman spectra are given in Figs. S2 and S3 for the neutral and cation P, Si, Al, and Zn doped boron clusters, and electronic densities of states in Fig. S4 in Supplementary Information. These can be used to compare with experimental results when these become available.

The dipole moments of the low lying doped boron clusters have also been calculated. B₆P₂, B₇P and B₈Si have relatively small dipole moments of 0.71 D, 0.31 D, 0.61 D; while the AlB₉ and ZnB₁₀ clusters have high dipole moments of 3.09 D and 2.00 D, respectively. The integrated atomic charges computed by AIMAll are shown in Table 2. The dipole moment has major contribution from charge redistribution in these doped clusters as well as the symmetry of the atomic structure. Clusters with inversion symmetry have zero dipole moments. The variation of the dipole moment amongst the doped clusters is correlated with the integrated atomic charges. For B₇P and B₆P₂ there is very little charge transfer between P and B atoms, but in B₈Si there is significant charge transfer from Si to B atoms. The excess charge is distributed equally over all the boron atoms. There is also significant charge transfer in B₁₀Zn, but the charge transfer from Zn is not distributed equally over all the boron atoms, and the symmetry is reduced, leading to a high net dipole moment. Large charge transfer from Al to B atoms is also obtained in B₉Al. The ionization potential (I.P.) has been calculated using Gaussian 09 (Table 1). B₈Si has the highest I.P. of 9.03 eV which is consistent with the fact that B₈Si also has the highest HOMO-LUMO gap amongst all the doped boron clusters we have studied. Zinc-doped boron cluster has the lowest I.P. (6.72 eV) and also the lowest HOMO-LUMO gap amongst

the low lying doped boron clusters. We also studied the anion clusters using Gaussian 09. The adiabatic and vertical detachment energies (ADE and VDE) of the neutral doped boron clusters show that B₇P (B₈Si) have low ADE and VDE of 0.72 (0.95) eV and 1.16 (1.96) eV, respectively, due to the closed electronic shell structure. These can be compared with photoelectron spectroscopy data when it becomes available.

AdNDP analysis has been performed to complement the understanding of the nature of bonding in doped boron clusters. In Fig. 12, we have shown the analysis for B₇P. Figure 12(a) shows the atomic structure, while in Fig. 12(b) the lone pair on P atom is seen. Thus effectively three p electrons on P participate in bonding, as discussed above. As also inferred from the analysis of the density distribution, Laplacian, and ELF, we obtain 6 two-center two-electron covalent bonds as shown in Fig. 12(c). AdNDP analysis produces six eight-center two-electron bonds corresponding to 12 delocalized electrons as discussed above. A similar analysis has been performed for B₈Si and is shown in Fig. 13; the atomic structure is shown in Fig. 13 (a), while Fig. 13 (b) shows a lone pair on Si so that only the p electrons participate in bonding. There are seven two center 2-electron sigma bonds between the neighboring boron atoms in the base, and six delocalized 9-center bonds have 12 electrons, corresponding to electronic shell closing as discussed above.

4. Conclusion

Multi-center bonding is generally discussed either within an orbital framework, in terms of canonical orbitals, or in terms of density matrix partitioning through the NBO and AdNDP schemes. Here we have presented another viewpoint from the analysis of the electronic charge density. This analysis shows that the concept of multi-center bonding appears even upon consideration of the total electron density. One does not have to rely on the orbital approximation or resort to a somewhat arbitrary partitioning into overlapping n-center 2-electron bonds. Furthermore, the multi-center delocalization seen in the Laplacian distribution does not refer to individual electrons, but to the total electron density. Since electrons are indistinguishable, it is not rigorously justifiable to regard some electrons as localized and others as delocalized over multiple atomic centers. The analysis in terms of the total electron density, its Laplacian and ELF avoids this conundrum. AdNDP analysis is also based on the concept of the electron pairing, but the emphasis is on partitioning the density to obtain the correct number of electron pair bonds that add up to the total electron count. When the analysis is in terms of the total electron density, this is trivially guaranteed by the fact that the latter integrates to the total number of electrons in the system.

As shown by Bader and Heard [14], the Laplacian of the electron density is generally homeomorphic to that of the conditional same spin pair density. The conditional same-spin pair density (for a fixed

position of the reference electron) can be expressed as the sum of the electron density of that spin and the density of the Fermi hole (a negative quantity) for that same spin. The Fermi hole density has been used to construct localization/delocalization measures [31-40], such as the localization index by integrating over the basin of a single atom and the delocalization index by integrating over the basin of a pair of atoms. The conditional same spin pair density is also related to ELF. Thus it is not surprising that while specific topological features of the Laplacian or of ELF may be sensitive to geometrical and computational artefacts, combination of topological analysis with information about the magnitudes of the density and its Laplacian can reveal fresh insights into electron localization/delocalization and the nature of chemical bonding in unusual systems. Analysis in terms of orbitals, bonds and total electron density can thus effectively complement each other. The delocalization index has been extensively used to construct aromaticity measures [31, 41-44]. The connection between magic clusters and aromatic stabilization is thus more than coincidental. Extension of the concept of aromaticity to boron clusters has been the subject of much study and debate in recent years [33, 34, 45-47].

Besides the nature of bonding we showed the magic nature of B_9^- and B_{10} clusters, which correspond to effectively 12 delocalized electrons. Also interestingly we found a high spin state of B_6^- to be the lowest energy state. We also studied doping of the pure boron clusters with C, P, Al, Si, and Zn atoms, and obtained doped clusters with large HOMO-LUMO gaps. Doping of atoms can thus be used to generate very stable species and to alter the properties of the pure clusters. The stability of these clusters has been correlated with effectively 12 delocalized electrons following a jellium model of a circular disk.

Acknowledgement

We gratefully acknowledge financial support from Shiv Nadar University and the use of the *Magus* high performance computing cluster. ABR and VK thankfully acknowledge financial support from International Technology Center – Pacific. We also thank the referees for careful and critical reading of the manuscript, and for many valuable comments and suggestions.

References:

- [1] Rahane AB and Kumar V 2015 *Nanoscale*. **7** 4055-62.
- [2] Zhai H-J, Zhao Y-F, Li W-L, Chen Q Bai H, Hu H-S *et al.* 2014 *Nature Chem.* **6** 727-31.
- [3] Zhao J, Wang L, Li F and Chen Z 2010 *J. Phys. Chem. A* **114** 9969-72.
- [4] Kato H, Yamashita K and Morokuma K 1993 *Bull. Chem. Soc. Japan* **66** 3358-61.
- [5] Oganov AR, Chen J, Gatti C, Ma Y, Ma Y, Glass CW, Liu Z, Yu T, Kurakevych OO, Solozhenko

VL 2009 *Nature*. **457** 863-7.

[6] Cheng L 2012 *J. Chem. Phys.* **136** 104301.

[7] Zubarev DY and Boldyrev AI 2008 *Phys. Chem. Chem. Phys.* **10** 5207-17.

[8] Jean Y, Volatron F and Burdett JK 1993 An introduction to molecular orbitals *Taylor & Francis USA*.

[9] Longuet-Higgins HC and Roberts MdV 1954 *Proc. Royal Soc. London A* **224** 336-47.

[10] Lipscomb WN 1973 *Acc. Chem. Res.* **6** 257-62.

[11] Wieczorek C, Allwohn J, Schmidt-Lukasch G, Hunold R, Massa W and Berndt A. 1990 *Angew. Chem.* **29** 398-9.

[12] Reed AE and Weinhold F 1983 *J. Chem. Phys.* **78** 4066-73.

[13] Bader RF. Atoms in molecules. John Wiley & Sons, Ltd; 1990.

[14] Bader RF, Heard GL 1999 *J. Chem. Phys.* **111** 8789-98.

[15] V. Kumar, *Comput. Mater. Sci.* 36, 1 (2006).

[16] Lv J, Wang Y, Zhang L, Lin H, Zhao J, Ma Y. 2015 *Nanoscale*. **7** 10482-9.

[17] Jian-Bing G, Xiang-Dong Y, Huai-Qian W and Hui-Fang L. 2012 *Chinese Phys. B* **21** 043102.

[18] Romanescu C, Galeev TR, Li W-L, Boldyrev AI and Wang L-S 2012 *Acc. Chem. Res.* **46** 350-8.

[19] Romanescu C, Galeev TR, Sergeeva AP, Li W-L, Wang L-S and Boldyrev AI 2012 *J. Organomet. Chem.* **721** 148-54.

[20] Reimann SM, Koskinen M, Häkkinen H, Lindelof PE and Manninen M 1997 *Phys. Rev. B* **56** 12147.

[21] Brack M 1993 *Rev. Mod. Phys.* **65** 677.

[22] Perdew JP, Burke K and Ernzerhof M 1996 *Phys. Rev. Lett.* **77** 3865.

[23] Kresse G and Furthmüller J 1996 *Comput. Mater. Sci.* **6** 15-50.

[24] Kresse G and Furthmüller J 1996 *Phys. Rev. B* **54** 11169.

[25] Gaussian 09, Rev.A.1, MJ Frisch, GW Trucks, HB Schlegel, GE Scuseria, MA Robb, JR Cheeseman, G. Scalmani, V. Barone, B. Mennucci, GA Petersson et al., Gaussian. Inc, Wallingford CT. 2009.

[26] Perdew JP, Burke K and Wang Y. 1996 *Phys. Rev. B* **54** 16533.

[27] Keith TA. AIMAll, TK Gristmill Software. Overland Park KS, USA. 2012.

[28] Sergeeva AP, Popov IA, Piazza ZA, Li W-L, Romanescu C, Wang L-S *et al* 2014 *Acc. Chem. Res.* **47** 1349-58.

[29] Tai TB, Grant DJ, Nguyen MT and Dixon DA 2009 *J. Phys. Chem. A* **114** 994-1007.

[30] Becke AD and Edgecombe KE 1990 *J. Chem. Phys.* **92** 5397-403.

[31] Sukumar N. 2012 A Matter of Density: Exploring the Electron Density Concept in the Chemical, Biological, and Materials Sciences. John Wiley & Sons, 83-88.

- [32] Carbó-Dorca R, Bultinck P. 2008 *J. Math. Chem.* **43** 1069-75.
- [33] Zhai HJ, Kiran B, Li J, Wang LS. 2003 *Nature Mater.* **2** 827-33.
- [34] Huang W, Sergeeva AP, Zhai HJ, Averkiev BB, Wang LS, Boldyrev AI. 2010 *Nature Chem.* **2** 202-6.
- [35] Feixas F, Matito E, Poater J, Solà M. 2015 *Chem. Soc. Rev.* **44** 6434-51.
- [36] Bader RF, Johnson S, Tang TH, Popelier PL. 1996 *J. Phys. Chem.* **100** 15398-415.
- [37] Matta CF, Hernández-Trujillo J, Bader RF. 2002 *J. Phys. Chem A.* **106** 7369-75.
- [38] Matta CF, Hernández-Trujillo J. 2003 *J. Phys. Chem A.* **107** 7496-504.
- [39] Hernández-Trujillo J, Matta CF. 2007 *Struct. Chem.* **18** 849-57.
- [40] Firme CL, Antunes OA, Esteves PM 2009 *Chem. Phys. Lett.* 2009 **468** 129-33.
- [41] Bader RF, Johnson S, Tang TH, Popelier PL. 1996 *J. Phys. Chem.* **100** 15398-415.
- [42] Matta CF, Bader RF. 2002 *Proteins: Structure, Function, Bioinf.* **48** 519-38.
- [43] Poater J, Fradera X, Duran M, Sola M. 2003 *Chem.–A Eur. J.* **9** 400-6.
- [44] Matito E, Poater J, Solà M, Duran M, Salvador P. 2005 *J. Phys. Chem A.* **109** 9904-10.
- [45] Hoffmann R 2015 *Amer. Sci.* **103** 18.
- [46] Ritter SK. 2015 Aromaticity by any other name. *C&E News online* **93**(8).
- [47] Xu C, Cheng L, Yang J. 2014 *J. Chem. Phys.* **141** 124301.

Table 1: Band gaps of Boron neutral clusters, anionic clusters and carbon doped clusters.

Neutral clusters	HOMO-LUMO gap (eV)	Anion clusters	HUMO-LUMO gap (eV)	Carbon doped boron clusters	HUMO-LUMO gap (eV)
B ₃	2.97	B ₃ ⁻	3.48	B ₂ C	3.40
B ₄	3.81	B ₄ ⁻	2.87	B ₃ C	2.93
B ₅	3.03	B ₅ ⁻	2.06	B ₄ C	1.94
B ₆	1.64	B ₆ ⁻	1.98 (quartet)	B ₅ C	2.22
B ₇	2.14	B ₇ ⁻	2.03	B ₆ C	1.50
B ₈	0.96	B ₈ ⁻	1.41	B ₇ C	2.08
B ₉	1.37	B ₉ ⁻	4.12	B ₈ C	3.43
B ₁₀	2.98	B ₁₀ ⁻	1.96	B ₉ C	2.16
B ₁₁	1.79	B ₁₁ ⁻	2.83		

Table 2: Dipole moment in Debye (D), ionization potential (I.P. in eV), integrated electron density on different atoms in the lowest energy isomer of doped boron clusters P, Al, and, Si doped boron clusters. The lowest energy isomer of B₁₀Zn is one in which a Zn atom caps the B₁₀ cluster.

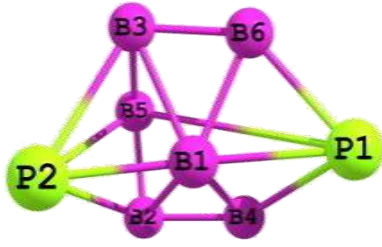
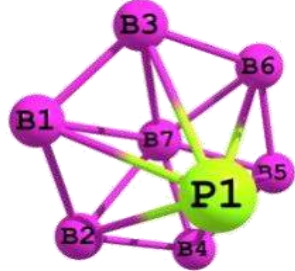
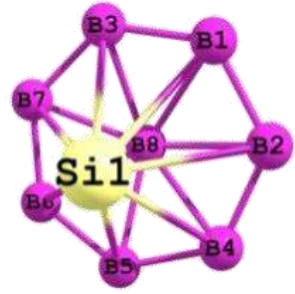
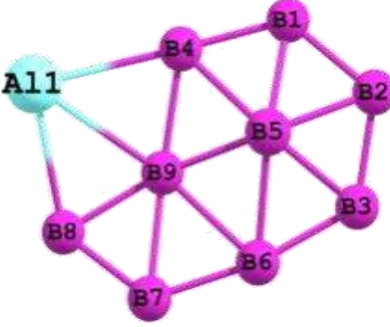
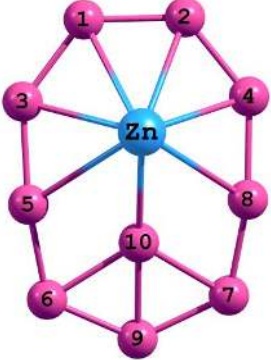
Cluster, Dipole moment	Ionization Potential	Cluster structure	Electron population of Atom
B ₆ P ₂ 0.71 D	8.962 eV		B1: 5.24 B2: 4.74 B3: 4.74 B4: 5.35 B5: 5.09 B6: 5.35 P1: 14.73 P2: 14.77
B ₇ P 0.31 D	8.762 eV		B1: 4.96 B2: 4.96 B3: 4.96 B4: 4.96 B5: 4.96 B6: 4.96 B7: 5.53 P1: 14.70
B ₈ Si 0.61 D	9.027 eV		B1: 5.06 B2: 5.06 B3: 5.06 B4: 5.06 B5: 5.06 B6: 5.06 B7: 5.06 B8: 5.25 Si1: 13.35
B ₉ Al 3.09 D	7.941 eV		B1: 4.98 B2: 4.94 B3: 4.95 B4: 5.36 B5: 5.32 B6: 4.96 B7: 4.96 B8: 5.40 B9: 5.46 Al1: 11.67
B ₁₀ Zn 3.29 D	7.773 eV		B1: 5.03 B2: 5.03 B3: 5.26 B4: 5.26 B5: 4.94 B6: 4.97 B7: 4.97 B8: 4.94 B9: 4.95 B10: 5.42 Zn1: 29.19

Figure Legends

Figure 1: Electron density contour plots of the lowest energy neutral boron clusters in the size range of 3 to 11 atoms, generated using AIMAll. Contour values: 0.001, 0.002, 0.004, 0.008, 0.02, 0.04, 0.08, 0.2, 0.4, 0.8, 2.0, 4.0, 8.0 e/Bohr³. The dark lines are bond paths (gradient paths of the electron density connecting pairs of nuclei). Boron nuclei are shown as pink spheres, bond critical points as green dots and ring critical points as red dots.

Figure 2: Contour plots of L for neutral boron clusters in the size range of 3 to 11 atoms, generated using AIMAll (Contour values: 0.0, ±0.001, ±0.002, ±0.004, ±0.008, ±0.02, ±0.04, ±0.08, ±0.2, ±0.4, ±0.8, ±2.0, ±4.0, ±8.0, ±20.0, ±40.0, ±80.0, ±200.0, ±400.0, ±800.0 e/Bohr⁵), overlaid with the bond paths, nuclear, bond and ring critical points. Positive contours of L (corresponding to regions of electron density accumulation) are shown as solid lines; negative contours of L (corresponding to regions of electron density depletion) are shown as dotted lines.

Figure 3: Electron density contour plots of the lowest energy anionic boron clusters in the range of 3 to 11 atoms, generated using AIMAll. Contour values as in Figure 1. The dark lines are bond paths (gradient paths of the electron density connecting pairs of nuclei). Boron nuclei are shown as pink spheres, bond critical points as green dots and ring critical points as red dots.

Figure 4: Contour plots of L for anionic boron clusters in the size range of 3 to 11 atoms, generated using AIMAll (contour value as in Figure 2), overlaid with the bond paths, nuclear, bond and ring critical points. Positive contours of L (corresponding to regions of electron density accumulation) are shown as solid lines; negative contours of L (corresponding to regions of electron density depletion) are shown as dotted lines.

Figure 5: ELF isosurfaces for neutral and anionic boron clusters in the size range of 3 to 11 atoms, generated using VASP at ELF isosurface 0.7.

Figure 6: Schematic structures of low energy isomers of boron clusters doped with a single carbon atom, B₃C to B₉C. The energies listed are relative to the isomer of lowest energy for each cluster size.

Figure 7: Electron density contour plots of carbon doped boron clusters, only the lowest energy isomer for each carbon doped cluster is shown; plots generated using AIMAll. Contour values as in Figure 1. The dark lines are bond paths (gradient paths of the electron density connecting pairs of nuclei). Boron nuclei are shown as pink spheres, carbon atoms as dark gray spheres, bond critical points as green dots and ring critical points as red dots.

Figure 8: Contour plots of L for carbon doped boron clusters, generated using AIMAll (contour value as in Figure 2), overlaid with the bond paths, nuclear, bond and ring critical points. Only the lowest energy isomer for each cluster size is shown. Positive contours of L (corresponding to regions of electron density accumulation) are shown as solid lines; negative contours of L (corresponding to regions of electron density depletion) are shown as dotted lines.

Figure 9: ELF isosurfaces for carbon doped boron clusters, generated using VASP at ELF isosurface 0.7.

Figure 10: Electron density contour plots of boron clusters doped with phosphorus, silicon, aluminum and zinc. Plots generated using AIMAll. Contour values as in Figure 1. The dark lines are bond paths (gradient paths of the electron density connecting pairs of nuclei). Boron, phosphorus, silicon,

aluminum, and zinc nuclei are shown as grey spheres while boron is shown as a pink sphere, bond critical points as green dots and ring critical points as red dots.

Figure 11: Contour plots of L for boron clusters doped with phosphorus, silicon, aluminum and zinc, generated using AIMAll (contour value as in Figure 2), overlaid with the bond paths, nuclear, bond and ring critical points. Positive contours of L (corresponding to regions of electron density accumulation) are shown as solid lines; contours of L (corresponding to regions of electron density depletion) are shown as dotted lines.

Figure 12: AdNDP analysis for B_7P . (a) Geometry (b) lone pair on P (c) six 2c-2e bonds (d)-(i) six 8c-2e bonds.

Fig. 13. AdNDP analysis for B_8Si . (a) Geometry (b) lone pair on Si (c) seven 2c-2e covalent bonds and (d)-(i) six 9c-2e bonds. Light blue spheres correspond to B atoms, while brown spheres correspond to Si atoms.

Figure S1: Electron densities at bond and ring critical points for (a) $B_3 - B_{11}$, (b) $B_3^- - B_{11}^-$, and (c) B_3C , B_4C , and B_5C .

Figure S2. IR and Raman spectra for neutral boron clusters doped with phosphorus, silicon, aluminum and zinc.

Figure S3. IR and Raman spectra for P, Si, Al, and Zn doped cation boron clusters.

Figure S4. Density of states for P, Si, Al, and Zn doped neutral boron clusters.

Figure S5: Electron density versus L at bond and ring critical points for (a) neutral and (b) anionic boron clusters in the size range of 3 to 11 atoms.

Figure S6: L at bond critical points versus bond ellipticities for (a) neutral and (b) anionic boron clusters in the size range of 3 to 11 atoms.

Figure S7: Correlation between the electron density and the Laplacian at BCPs of B-B bonds in carbon-doped neutral boron clusters.

Figure 1

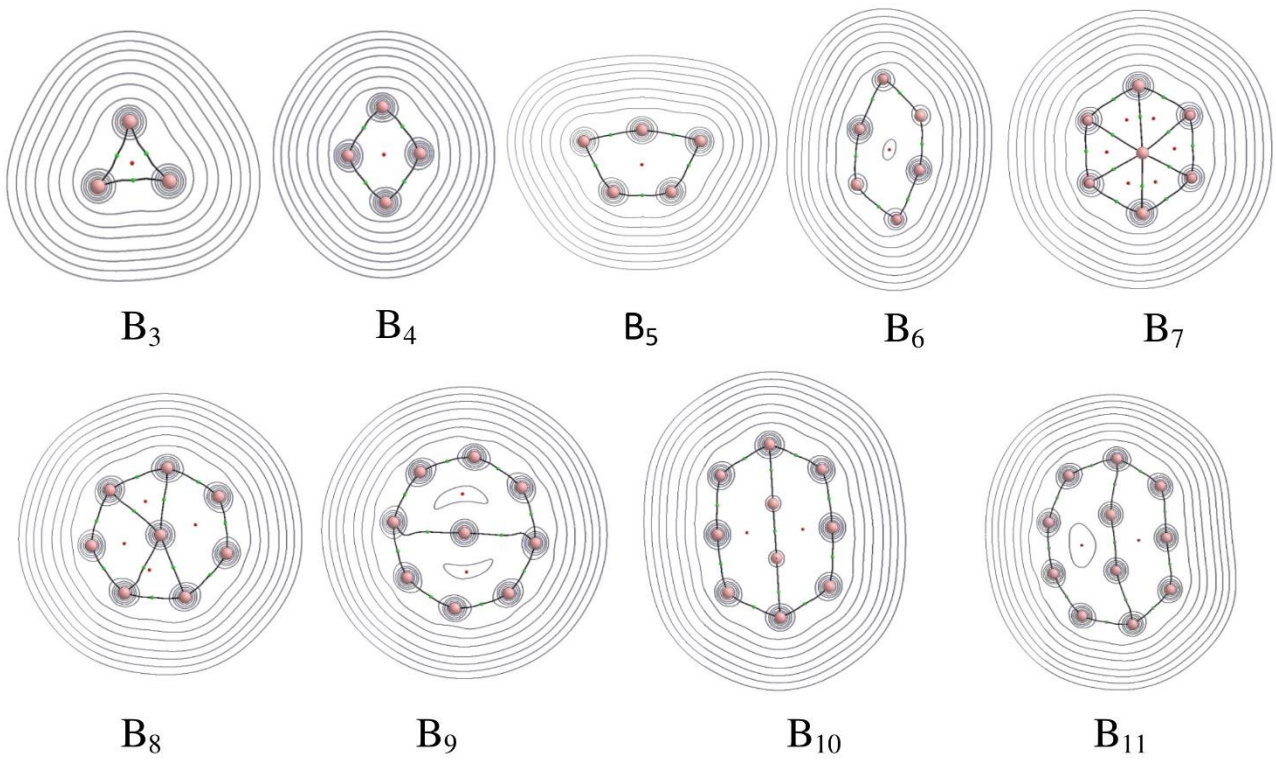
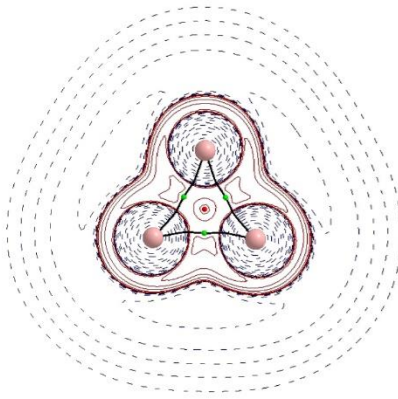
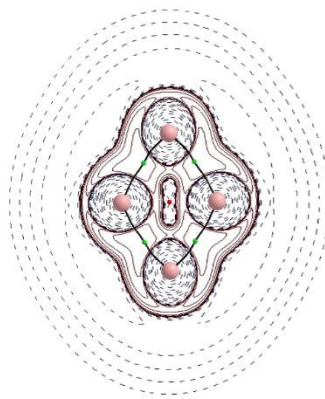


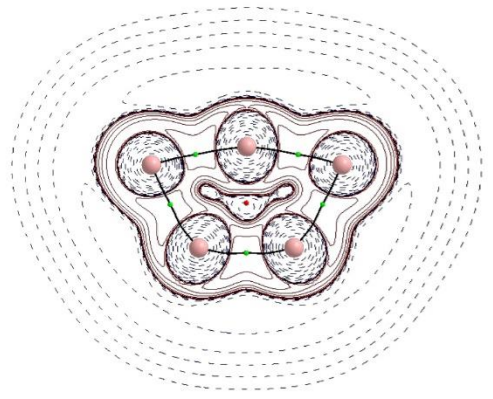
Figure 2



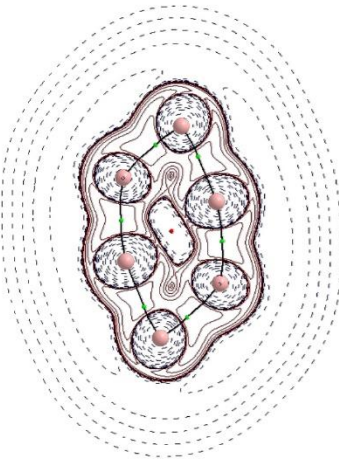
B₃



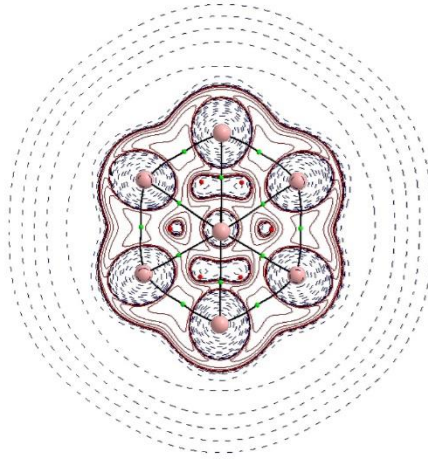
B₄



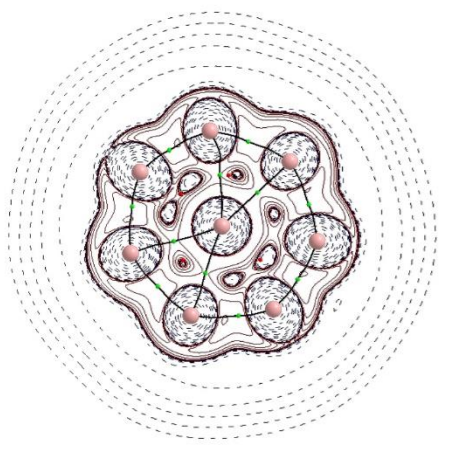
B₅



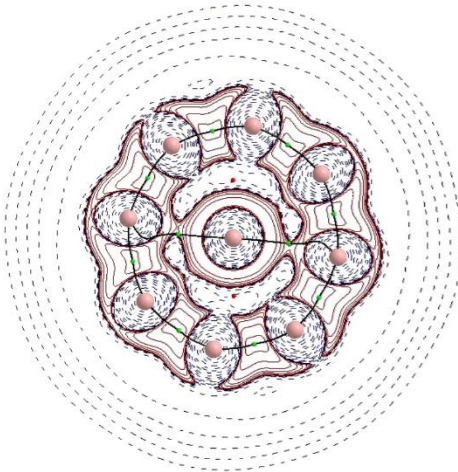
B₆



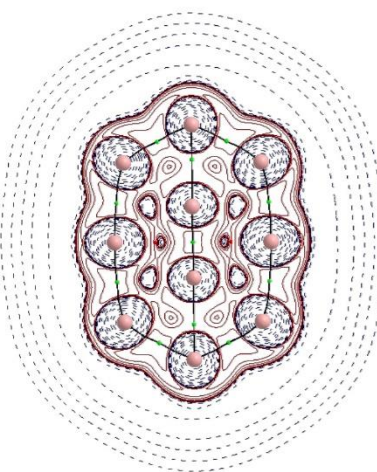
B₇



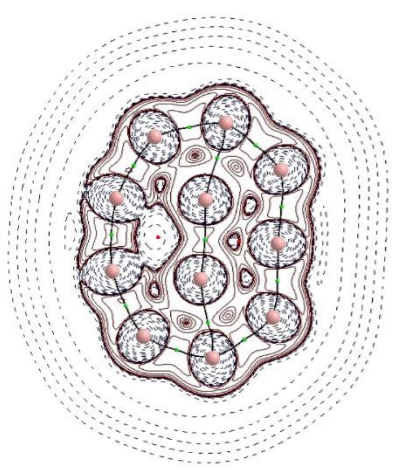
B₈



B₉



B₁₀



B₁₁

Figure 3

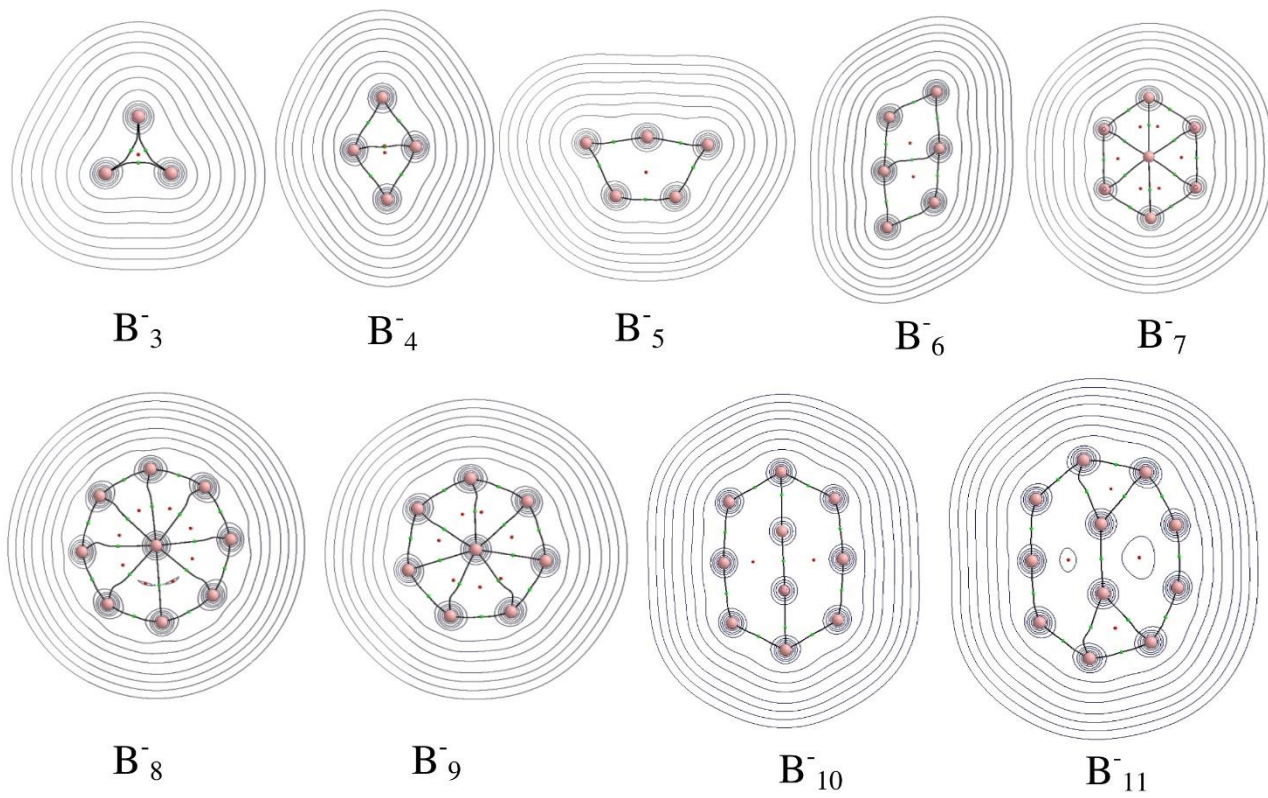
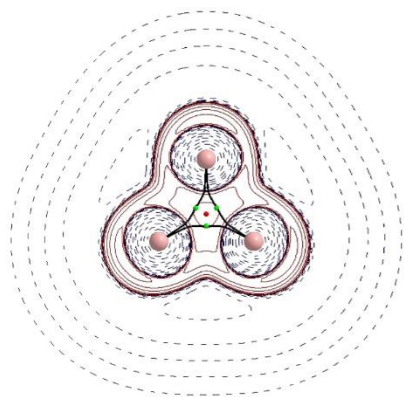
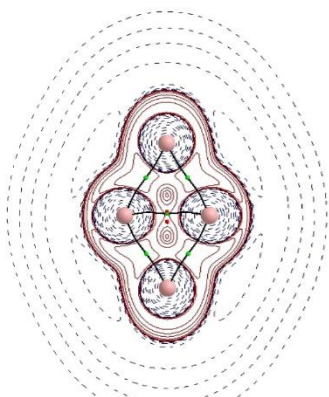


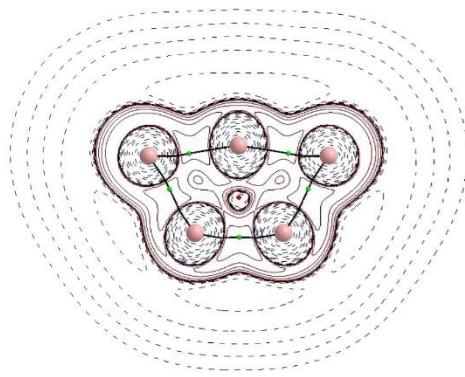
Figure 4



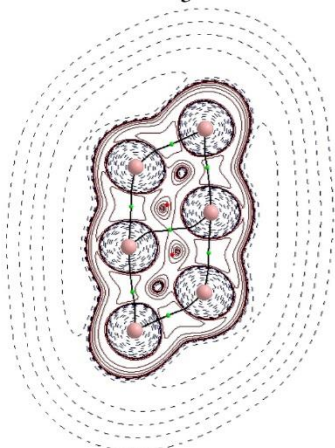
B_3^-



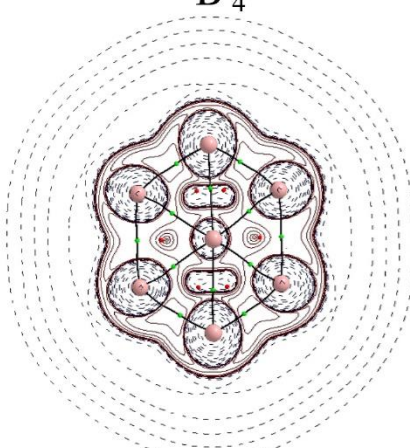
B_4^-



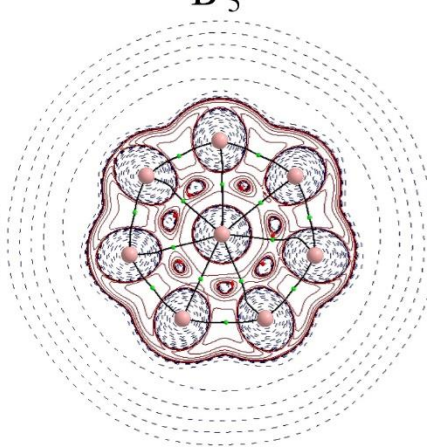
B_5^-



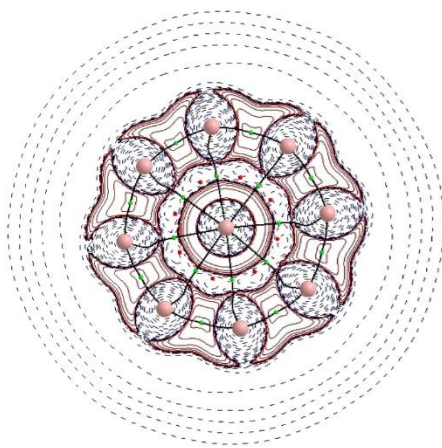
B_6^-



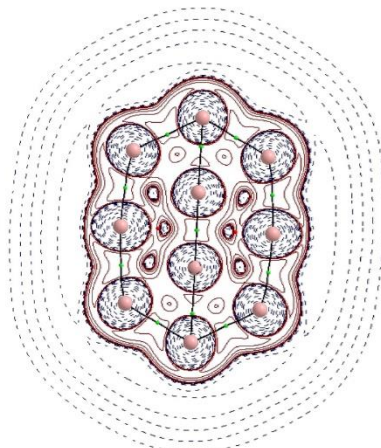
B_7^-



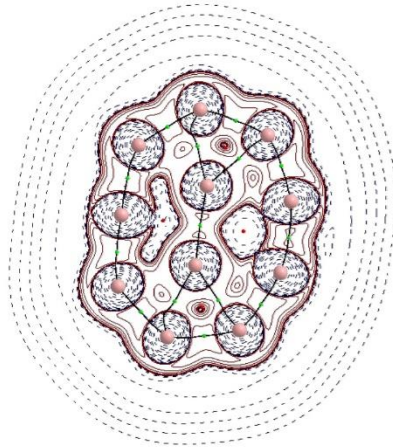
B_8^-



B_9^-



B_{10}^-



B_{11}^-

Figure 5

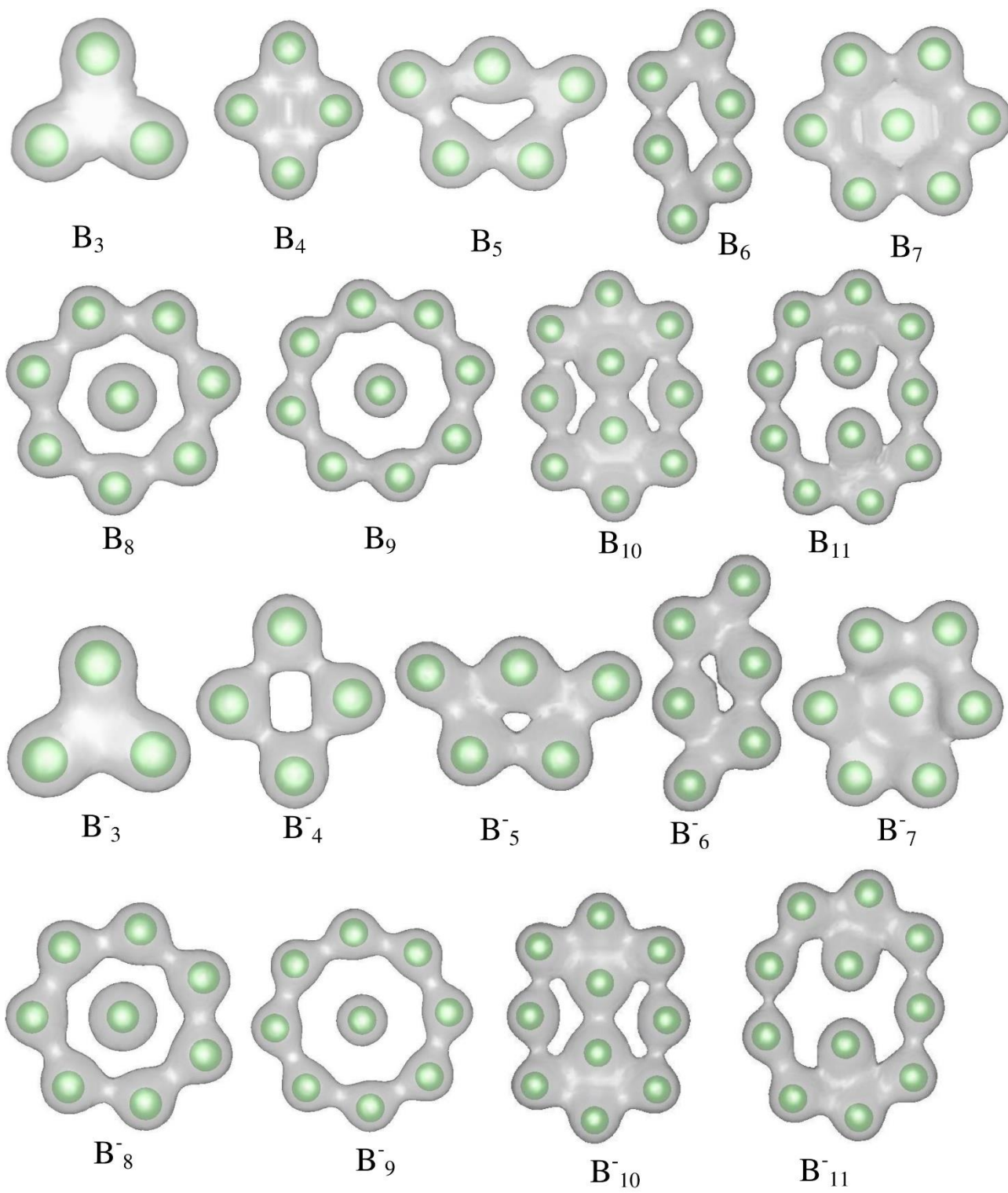


Figure 6

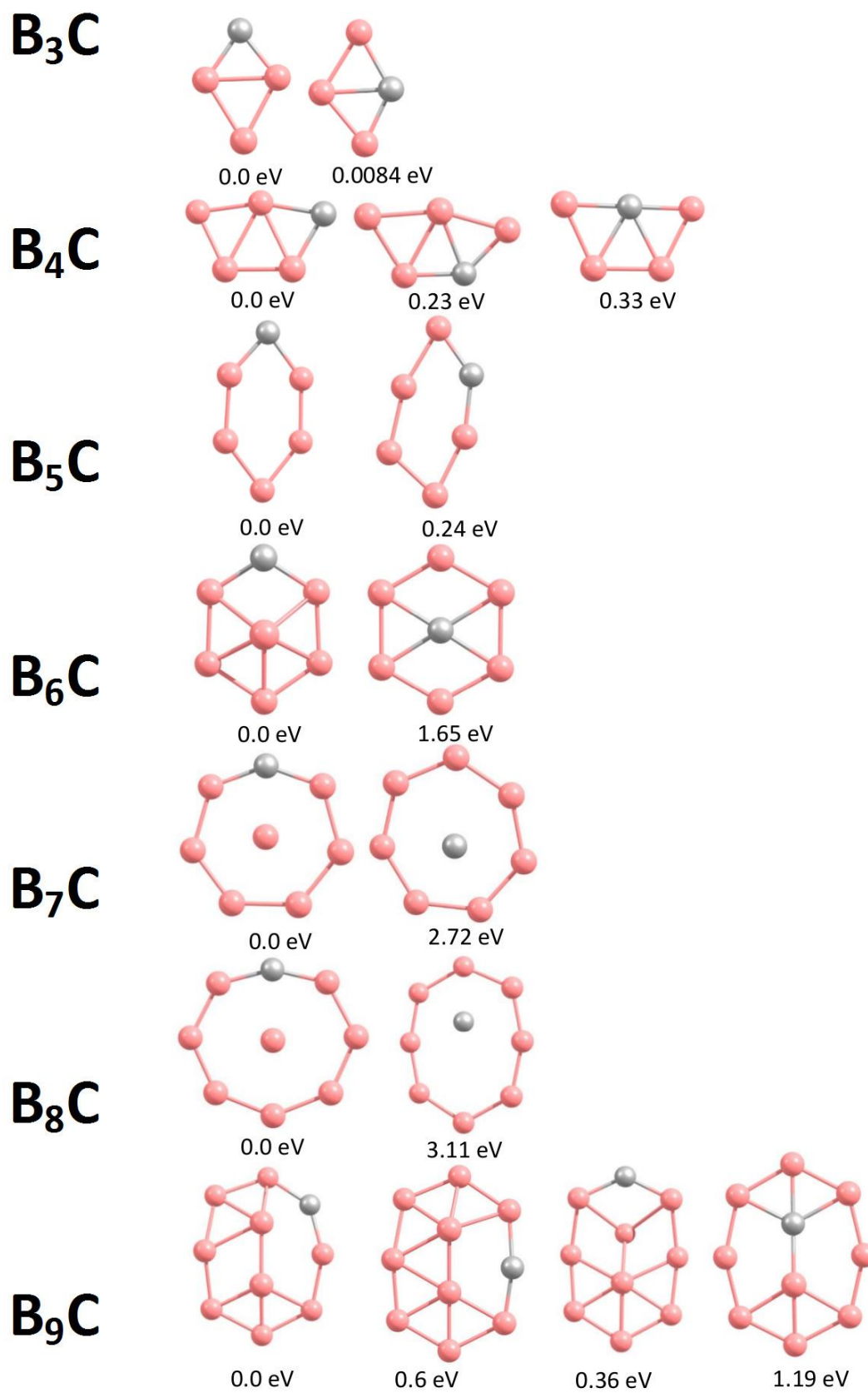
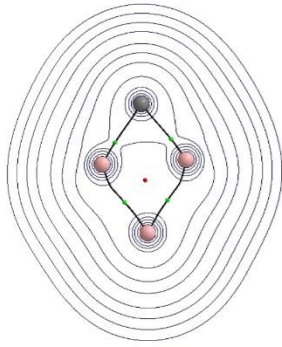
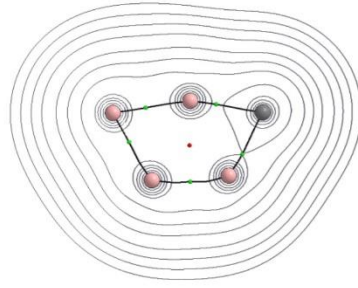


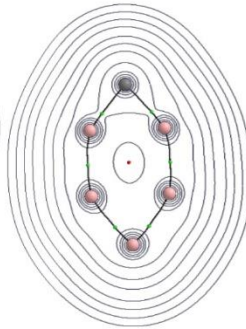
Figure 7



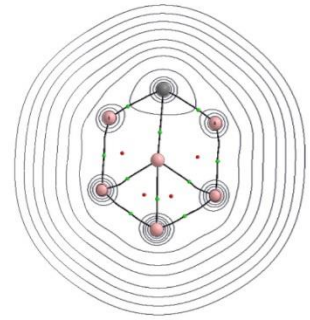
B_3C



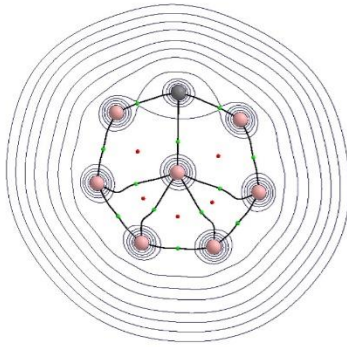
B_4C



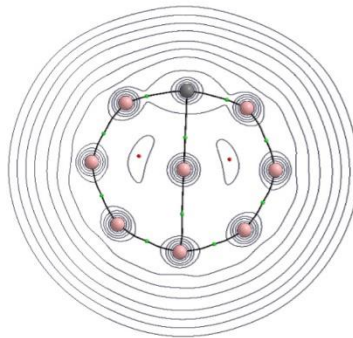
B_5C



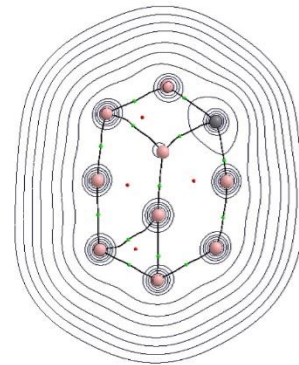
B_6C



B_7C



B_8C



B_9C

Figure 8

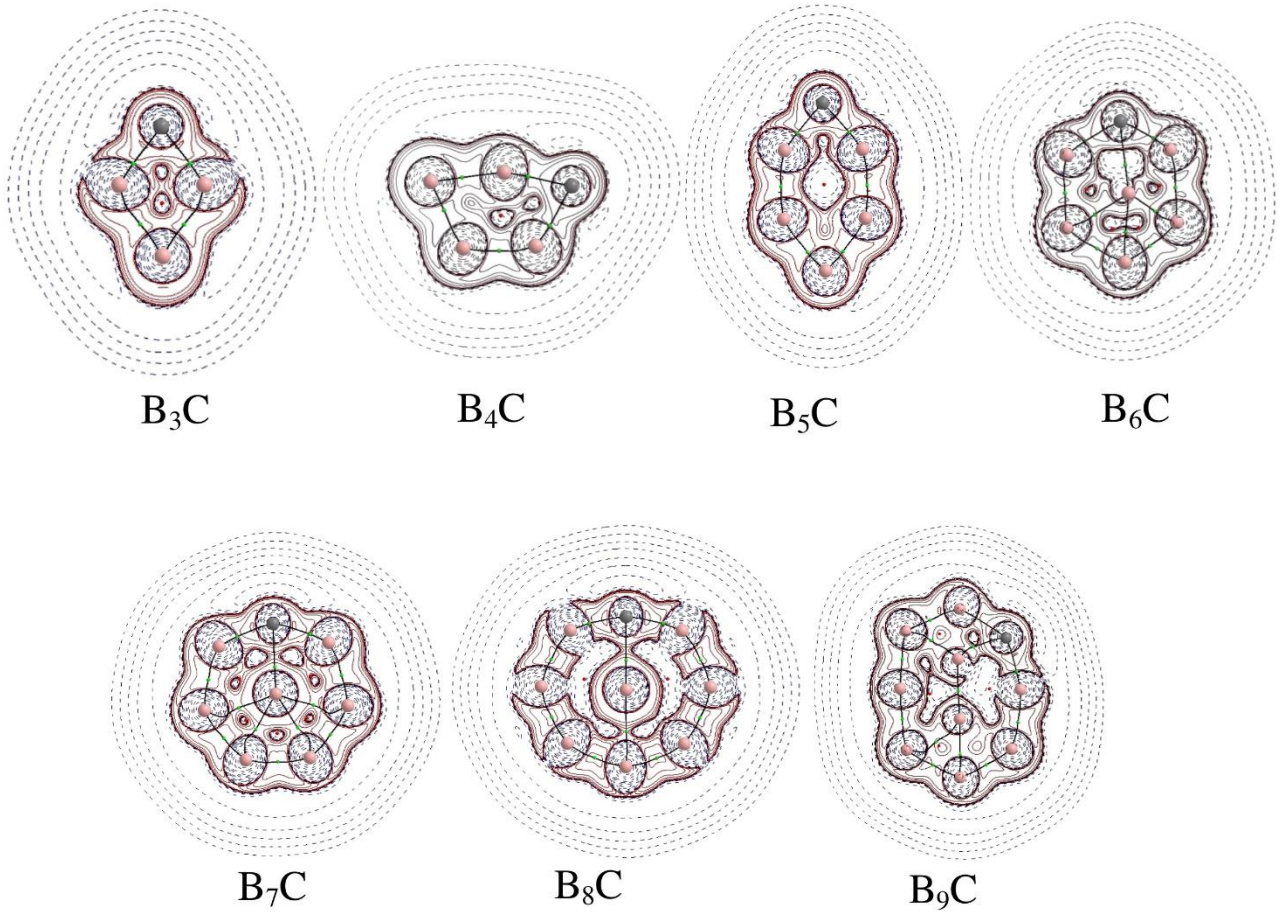


Figure 9

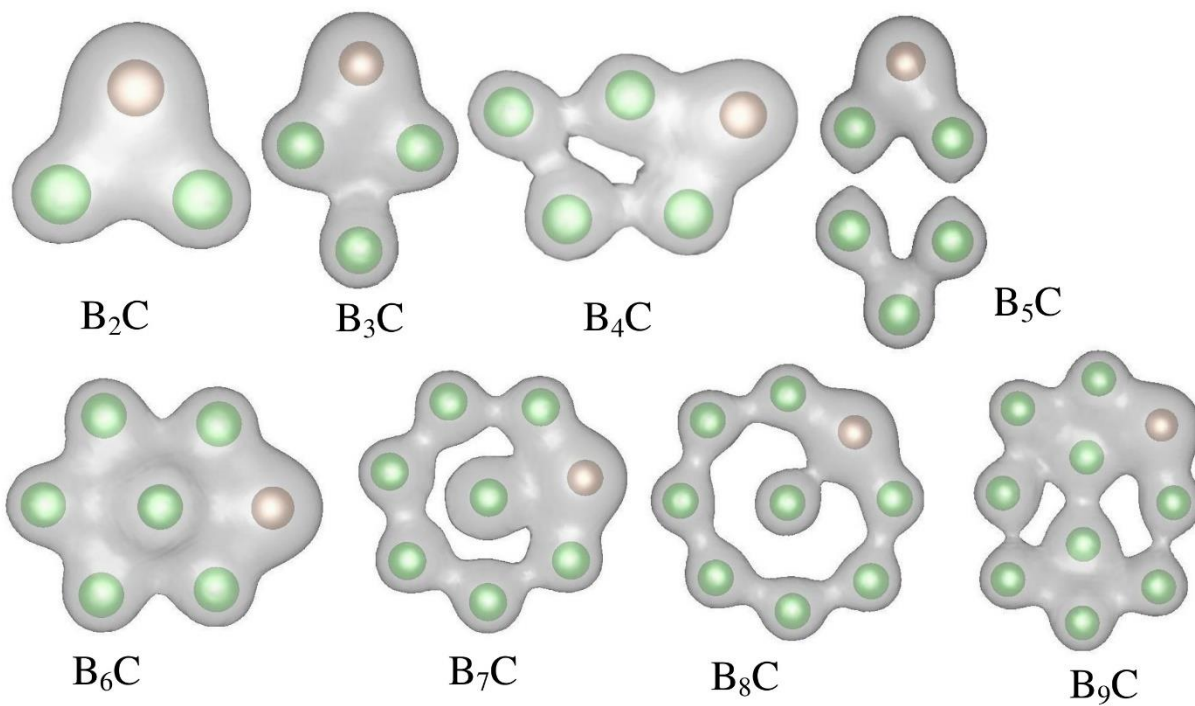
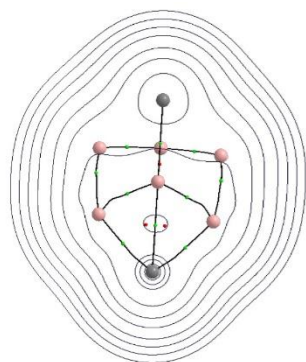
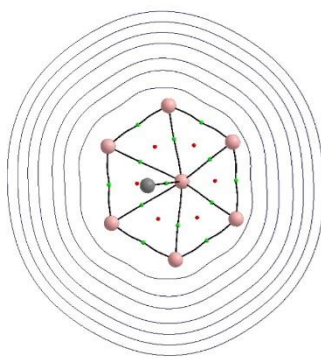


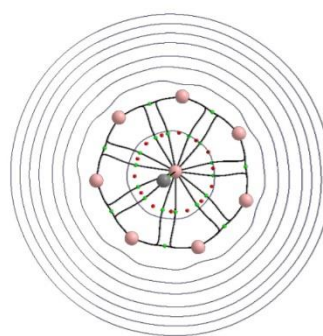
Figure 10



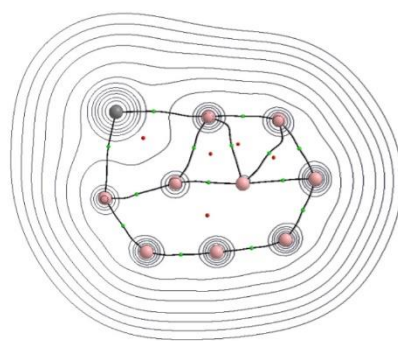
B_6P_2



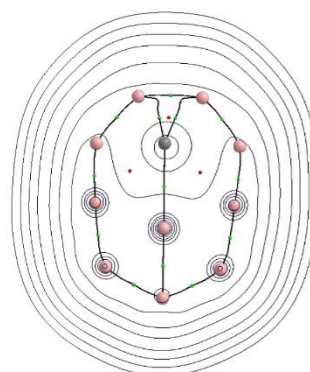
B_7P



B_8Si



B_9Al



$B_{10}Zn$

Figure 11

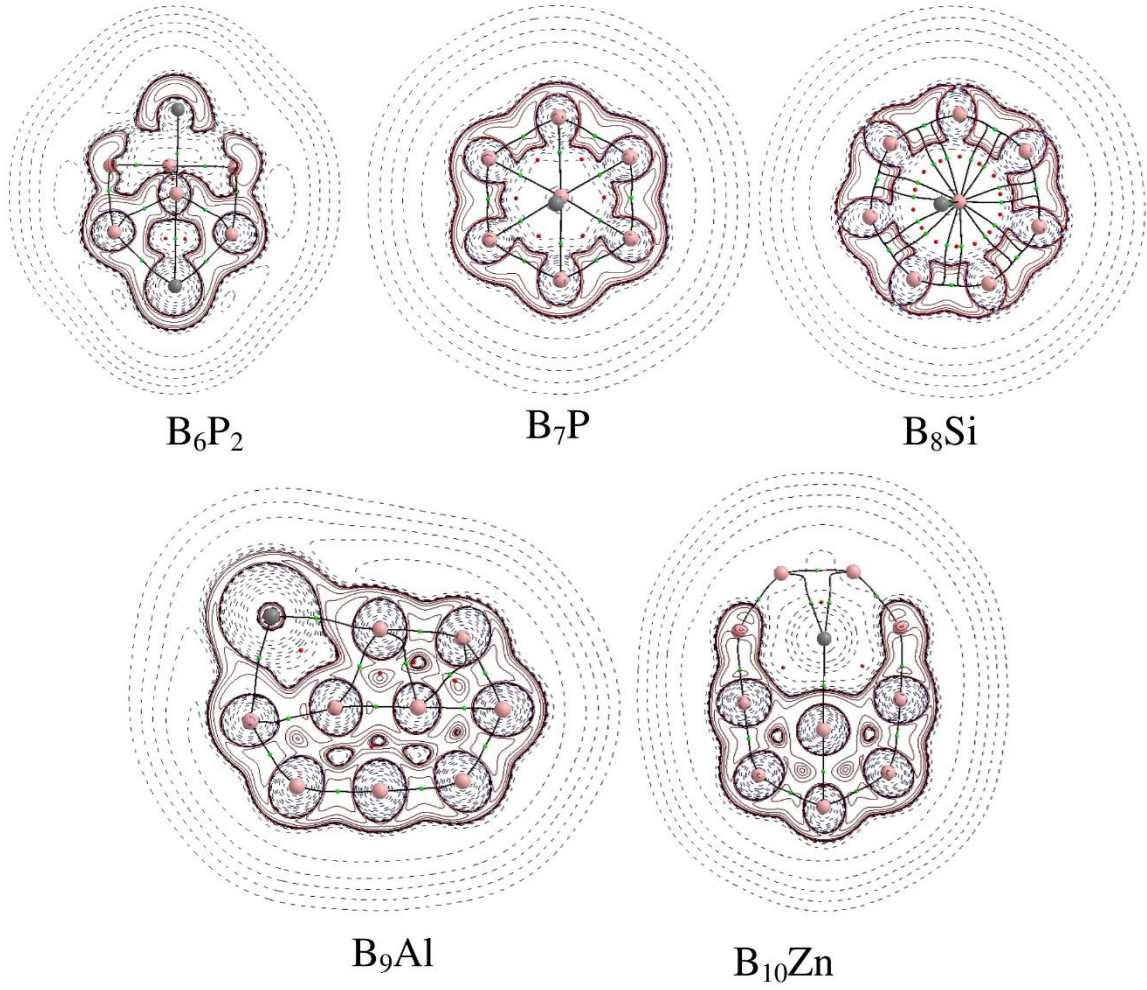


Figure 12

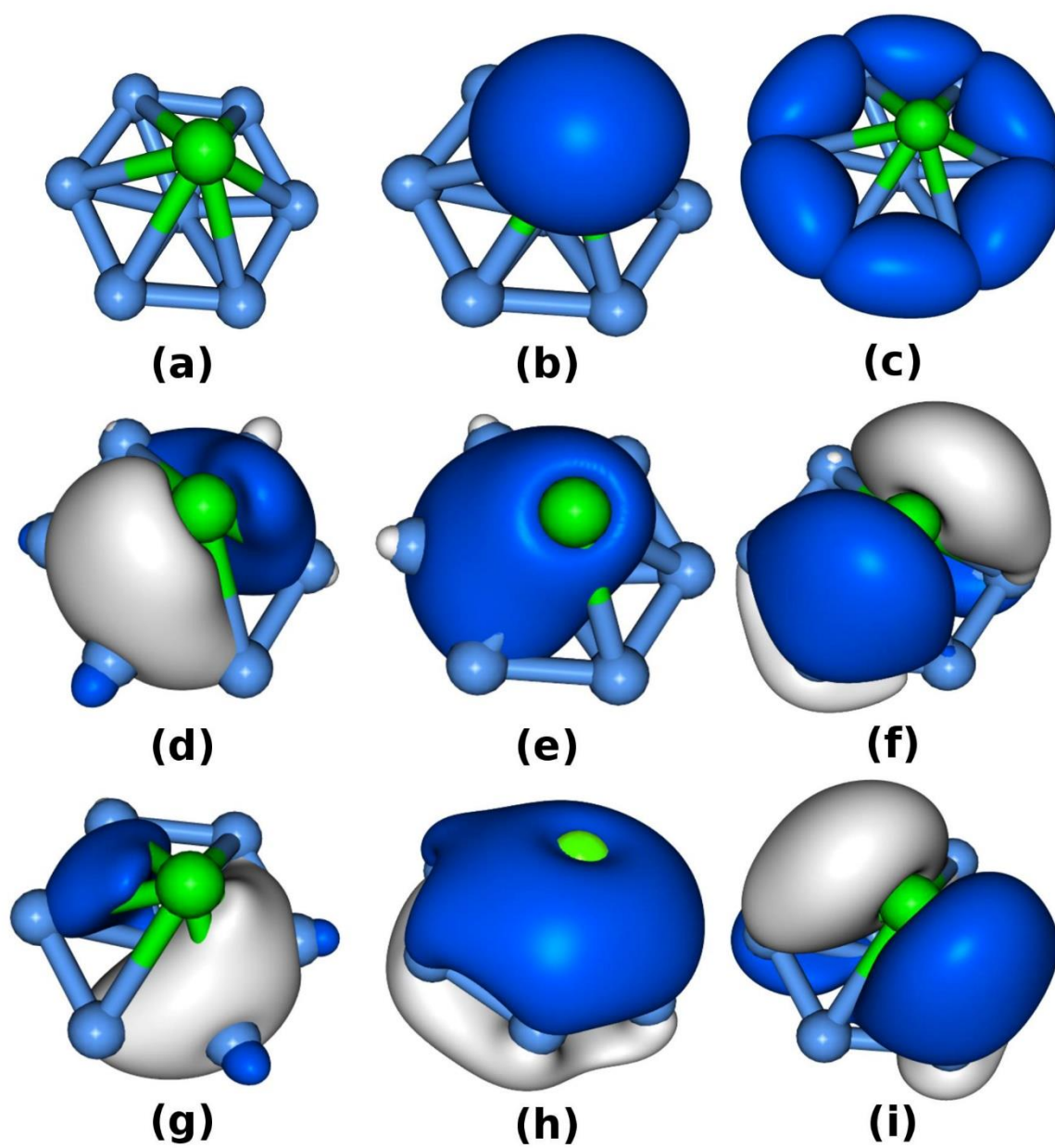


Figure 13

